Supplementary Information for: Observing the dynamics of quantum states generated inside nonlinear optical cavities

Seou Choi[‡,1],[*] Yannick Salamin[‡,1,2,3],[†] Charles Roques-Carmes[1,4], Jamison Sloan[1,4], Michael Horodynski[2], and Marin Soljačić[1,2]

[‡] *denotes equal contribution.*

[1] *Research Laboratory of Electronics, Massachusetts Institute of Technology, Cambridge, MA 02139, USA*

[2] *Department of Physics, Massachusetts Institute of Technology, Cambridge, MA 02139, USA*

[3] *CREOL, The College of Optics and Photonics, University of Central Florida, Orlando, Florida 32816, USA and*

[4] *E. L. Ginzton Laboratories, Stanford University, 348 Via Pueblo, Stanford, CA USA*

[*]Electronic address: seouc130@mit.edu

[†]Electronic address: yannick.salamin@ucf.edu

Contents

S1. VISUALIZING CAVITY QUANTUM STATES

Before we discuss the cavity quantum state reconstruction protocol, we first introduce how we can visualize theses states in 2D phase space.

A. Quantum state representation on phase space

The Glauber-Sudarshan P function is the classical correspondence of the density matrix ρ. ρ is expanded as a diagonal sum over coherent states [1]:

$$\rho = \int d^2\alpha \, |\alpha\rangle \langle\alpha| \, P(\alpha, \alpha^*). \tag{S1}$$

The over-completeness of the coherent state allows ρ to be represented as a quasi-probability distribution on a continuous 2D phase space as below:

$$\begin{aligned} \int P(\alpha, \alpha^*) d^2\alpha &= \int P(\alpha, \alpha^*) \, \langle\alpha|\alpha\rangle \, d^2\alpha \\ &= tr\left(\int |\alpha\rangle \langle\alpha| \, P(\alpha, \alpha^*) d^2\alpha \right) \\ &= tr(\rho) \\ &= 1. \end{aligned} \tag{S2}$$

Another phase space representation is the Husimi Q function, which gives the probability of observing a certain coherent state $|\alpha\rangle$ for a given quantum state $|\psi\rangle$.

$$\begin{aligned} Q(\alpha, \alpha^*) &= \frac{1}{\pi} \langle\alpha|\rho|\alpha\rangle \\ &= \frac{1}{\pi} |\, \langle\alpha|\psi\rangle \,|^2. \end{aligned} \tag{S3}$$

In this paper, we mainly use the Husimi Q function to visualize the actual quantum state, and the Glauber-Sudarshan P function to derive bias – probability relationship. The P function can be converted to the Q function using the following equation [1]:

$$Q(\alpha, \alpha^*) = \frac{1}{\pi} \int P(\beta, \beta^*) e^{-|\beta-\alpha|^2} d^2\beta. \tag{S4}$$

S2. CAVITY QUANTUM STATE RECONSTRUCTION PROTOCOL

This section describes how we can reconstruct the Husimi Q function of a degenerate optical parametric oscillator (DOPO) quantum state. We will show how the bias field displaces the cavity quantum state, resulting in a change in the probability of measuring a DOPO steady state. By calculating the sensitivity of the probability to the applied bias field, we can reconstruct the Husimi Q function. To validate our reconstruction protocol, we perform numerical experiments in reconstructing three different DOPO quantum states.

A. Displacing quantum states with bias field

We can write the Fokker-Planck equation of the DOPO state, which is the semi-classical correspondence of the Heisenberg-Langevin equation describing the time evolution of the P function [2]:

$$\begin{aligned}\frac{\partial}{\partial\tau}P(\alpha,\alpha^*) = \Bigg\{ &\frac{\partial}{\partial\alpha}\left[\alpha - b - \left(\lambda - g^2\alpha^2\right)\alpha^*\right] + \frac{\partial}{\partial\alpha^*}\left[\alpha^* - b^* - \left(\lambda - g^2\alpha^{*2}\right)\alpha\right] \\ &+\frac{1}{2}\left[\frac{\partial^2}{\partial\alpha^2}\left(\lambda - g^2\alpha^2\right) + \frac{\partial^2}{\partial\alpha^{*2}}\left(\lambda - g^2\alpha^{*2}\right)\right]\Bigg\}P(\alpha,\alpha^*).\end{aligned} \tag{S5}$$

Here, τ is the time normalized by the cavity lifetime, b denotes the bias field, λ is the ratio of the pump field above threshold, and g^2 quantifies the quantum noise level [2]. The corresponding classical stochastic differential equations (SDEs) are:

$$\begin{aligned}d\alpha &= (b - \alpha + \alpha^*(\lambda - g^2\alpha^2))d\tau + \sqrt{\lambda - g^2\alpha^2}dW_\alpha \\ d\alpha^* &= (b^* - \alpha^* + \alpha(\lambda - g^2\alpha^{*2}))d\tau + \sqrt{\lambda - g^2\alpha^{*2}}dW_{\alpha^*}.\end{aligned} \tag{S6}$$

Here, dW_{α,α^*} are Gaussian noise increments satisfying $\langle dW_i(t)dW_j(t')\rangle = \delta_{ij}\delta(t-t')$.

For macroscopic DOPO systems, $g \ll 1$, allowing us to neglect the nonlinear term until the system has enough photons to induce strong nonlinear absorption [2]. With $X = (\alpha + \alpha^*)/\sqrt{2}$, $Y = (\alpha - \alpha^*)/\sqrt{2}i$, and assuming a real b, we can rewrite Supplementary Equation S6 as:

$$\begin{bmatrix} \frac{dX}{d\tau} \\ \\ \frac{dY}{d\tau} \end{bmatrix} = \begin{bmatrix} -1+\lambda & 0 \\ \\ 0 & -1-\lambda \end{bmatrix} \begin{bmatrix} X \\ \\ Y \end{bmatrix} + \begin{bmatrix} \sqrt{2}b \\ \\ 0 \end{bmatrix} + \sqrt{\lambda} \begin{bmatrix} \eta_X \\ \\ \eta_Y \end{bmatrix}. \tag{S7}$$

where $\eta_{X,Y}$ are independent Gaussian noises. We focus on the amplifying quadrature X when discussing the displacement of the cavity state, which corresponds to Equation 4 of the main text.

B. Reconstructing the Husimi Q function

In the main text, we described how the Husimi Q function of the cavity quantum state can be reconstructed by analyzing the statistics of cavity steady states after applying a displacement. We also highlighted that the displacement of the cavity quantum state depends on the phase of the pump field. Here, we validate our claim that our displacement theorem holds for an arbitrary pump phase. For the pump field with amplitude λ and phase ϕ,

$$\begin{aligned} d\alpha &= (b - \alpha + \alpha^*(\lambda e^{i\phi} - g^2\alpha^2))d\tau + \sqrt{\lambda e^{i\phi} - g^2\alpha^2}dW_\alpha \\ d\alpha^* &= (b^* - \alpha^* + \alpha(\lambda e^{-i\phi} - g^2\alpha^{*2}))d\tau + \sqrt{\lambda e^{-i\phi} - g^2\alpha^{*2}}dW_{\alpha^*}. \end{aligned} \tag{S8}$$

For $g \ll 1$, we can simplify Supplementary Equation S8:

$$\begin{bmatrix} \frac{dX}{d\tau} \\ \\ \frac{dY}{d\tau} \end{bmatrix} = \begin{bmatrix} \lambda\cos\phi - 1 & \lambda\sin\phi \\ \\ \lambda\sin\phi & -\lambda\cos\phi - 1 \end{bmatrix} \begin{bmatrix} X \\ \\ Y \end{bmatrix} + \sqrt{2} \begin{bmatrix} \mathrm{Re}(b) \\ \\ \mathrm{Im}(b) \end{bmatrix} + \sqrt{\lambda} \begin{bmatrix} \cos\frac{\phi}{2} & -\sin\frac{\phi}{2} \\ \\ \sin\frac{\phi}{2} & \cos\frac{\phi}{2} \end{bmatrix} \begin{bmatrix} \eta_X \\ \\ \eta_Y \end{bmatrix}. \tag{S9}$$

We rotate the coordinates to diagonalize the drift term using:

$$\begin{bmatrix} \tilde{Y} \\ \\ \tilde{X} \end{bmatrix} = \begin{bmatrix} \sin\frac{\phi}{2} & -\cos\frac{\phi}{2} \\ \\ \cos\frac{\phi}{2} & \sin\frac{\phi}{2} \end{bmatrix} \begin{bmatrix} X \\ \\ Y \end{bmatrix}. \tag{S10}$$

This rotation transforms Supplementary Equation S9 into a new coordinate system as:

$$\begin{bmatrix} \frac{d\tilde{X}}{d\tau} \\ \\ \frac{d\tilde{Y}}{d\tau} \end{bmatrix} = \begin{bmatrix} -1+\lambda & 0 \\ \\ 0 & -1-\lambda \end{bmatrix} \begin{bmatrix} \tilde{X} \\ \\ \tilde{Y} \end{bmatrix} + \begin{bmatrix} \sqrt{2}b_0 \\ \\ 0 \end{bmatrix} + \sqrt{\lambda} \begin{bmatrix} \eta_{\tilde{X}} \\ \\ \eta_{\tilde{Y}} \end{bmatrix}. \tag{S11}$$

Here, the bias field $b = b_0 e^{i\frac{\phi}{2}}$ ensures maximum displacement along the $\tilde{X}$-axis.

Supplementary Equation S11 is identical to Supplementary Equation S7, except that the amplification of DOPO signal happens along the quadrature which is rotated by $\phi/2$ (which is aligned to the phase of the bias field). Therefore, we can use Equation 7 in the main text to measure the marginal distributions of the Husimi Q function along the different quadrature phases ($\theta = \phi/2$). Finally, we perform the inverse Radon transform to reconstruct the full 2D Husimi Q function from multiple marginal distributions [3].

To validate our concept, we reconstructed the Husimi Q function of three different DOPO quantum states, which are quantum vacuum state, squeezed vacuum state and amplified quantum vacuum state. We numerically calculate the probability p by determining the area of the displaced Husimi Q function at a given quadrature phase θ and bias field b. We sweep the bias field b to obtain the sensitivity of the probability p to the bias field b, $\partial p/\partial b$, which corresponds to the marginal distribution of the Husimi Q function. We repeat this process for different pump phases to reconstruct the full 2D Husimi Q function. We compare the numerically reconstructed 2D Husimi Q function to the analytical solutions, shown in Supplementary Figure S1, and see that our reconstruction protocol works for all three different cases.

S3. STOCHASTIC DIFFERENTIAL EQUATIONS OF OPTICAL PARAMETRIC OSCILLATOR

Until now, we have described how we can reconstruct the Husimi Q function using the displacement theory. Although the displacement theory provides an intuitive framework for understanding how the relationship between the bias and probability can be used to reconstruct the cavity state, it is limited to the early dynamics of the OPO (i.e., during the linear amplification of the quantum state).

In this section, we introduce an alternative reconstruction protocol based on SDEs. We analytically solve SDEs for the biased OPO to derive the bias – probability relationship. Using this relationship, we reconstruct the Husimi Q function by calculating the sensitivity of the probability to the bias field. As a proof of concept, we perform a numerical experiment reconstructing two different dynamics of the DOPO: (1) the amplification of the quantum vacuum state to the steady states, and (2) the generation and subsequent collapse of the squeezed vacuum state.

A. Bias – probability relationship at nonlinear absorption stage

We now solve the SDE of a biased OPO to calculate the bias – probability relationship and reconstruct the Husimi Q function in the nonlinear absorption stage. The bias – probability relationship for the early dynamics of the DOPO can be found in the Methods section of the main text.

As the OPO signal grows and nonlinear absorption becomes dominant, the noise term can be ignored.

$$\dot{\alpha} = f(\alpha) \equiv (\lambda - 1)\alpha - g^2\alpha^3 + b. \tag{S12}$$

Here, $f(\alpha)$ indicates the momentum of the trajectory, and $f^{'}(\alpha)$ indicates its stability. $f(\alpha)$ has local extremes at $\alpha = \pm\alpha_{\mathrm{critical}} = \pm\alpha_0/\sqrt{3}$ (i.e., when $f'(\alpha) = 0$). We consider the non-trivial case where three real-valued solutions for α satisfy $f(\alpha) = 0$. The dynamics are then analyzed based on the value of α and their corresponding roles in determining the system's behavior.

Case I: $|\alpha| > \alpha_{\mathrm{critical}}$

For $|\alpha| > \alpha_{\text{critical}}$, $f^{'}(\alpha)$ is always negative, so α can reach a certain stable point. For $\alpha > \alpha_{\text{critical}}$, α approaches $+\alpha_0$, and $-\alpha_0$ for the opposite case.

Case II: $|\alpha| < \alpha_{\text{critical}}$

We define $\alpha_{\text{threshold}}$ as a point which satisfies $f(\alpha_{\text{threshold}}) = 0$ for $|\alpha| < \alpha_{\text{critical}}$. Because $f^{'}(\alpha) > 0$, α will bifurcate with respect to $\alpha_{\text{threshold}}$. For $\alpha > \alpha_{\text{threshold}}$, it will move towards α_{critical}, and since $f'(\alpha) < 0$ for $\alpha > \alpha_{\text{critical}}$, α will eventually reach $+\alpha_0$. Similarly, $\alpha < \alpha_{\text{threshold}}$ will reach $-\alpha_0$.

Based on the discussion above, we can conclude that $p = P(\alpha(\tau) > \alpha_{\text{threshold}})$. $\alpha_{\text{threshold}}$ is a function of b, $\alpha_{\text{threshold}} = h(b)$. Therefore, the relationship between the field probability distribution of the DOPO state $P(\alpha)$ and the bias-probability sensitivity $\partial p/\partial h(b)$ is given by:

$$P(\alpha = \alpha_{\text{threshold}}) = -\partial p/\partial h(b). \tag{S13}$$

The negative sign arises because $h(b)$ decreases as b and p increase. In our numerical simulations, we compute the probability p at different bias field b, then take the derivative with respect to $h(b)$ to calculate the field probability distribution.

Now, we discuss how we can derive the analytical solution of the bias – probability relationship. Before introducing the bias, the equation of motion for the unbiased OPO can be written as:

$$\dot{\alpha} = (\lambda - 1)\alpha - g^2\alpha^3. \tag{S14}$$

Note that the differential equation becomes deterministic because the noise term is neglected. Solving this equation, we get

$$\alpha(\tau) = \frac{\alpha_0\alpha(\tau_0)e^{(\lambda-1)(\tau-\tau_0)}}{\sqrt{\alpha^2(\tau_0)(e^{2(\lambda-1)(\tau-\tau_0)} - 1) + \alpha_0^2}}. \tag{S15}$$

τ_0 is defined as the time when the OPO transitions from the linear amplification stage and the nonlinear absorption stage.

From Supplementary Equation S15, we can rewrite $P(\alpha(\tau) > \alpha_{\text{threshold}})$ as

$$P\left[\alpha(\tau_0) > T(b) \equiv \frac{H(b)}{\sqrt{1+\frac{H^2(b)}{\alpha_0^2}}}\right], \quad H(b) \equiv \frac{h(b)e^{-(\lambda-1)(\tau-\tau_0)}}{\sqrt{1-\frac{h^2(b)}{\alpha_0^2}}}. \tag{S16}$$

Now we turn our attention to the linear amplification stage to calculate $P\left[\alpha(\tau_0)\right]$. The SDE for the linear amplification stage can be derived from Supplementary Equation S6 by setting $b = 0$. Here, we consider the real part of α and neglect the nonlinear term.

$$\dot{\alpha} = (\lambda - 1)\alpha + \sqrt{\lambda}\eta_\alpha. \tag{S17}$$

As an integral form,

$$\alpha(\tau) = \alpha(0)e^{(\lambda-1)\tau} + \int_0^\tau \sqrt{\lambda}e^{(\lambda-1)(\tau-t)}\eta_\alpha dt. \tag{S18}$$

The mean $\langle\alpha(\tau)\rangle$ and variance Var($\alpha(\tau)$) can be calculated from Supplementary Equation S18.

$$\begin{aligned} \langle\alpha(\tau)\rangle &= \langle\alpha(0)\rangle e^{(\lambda-1)\tau} \\ \text{Var}(\alpha(\tau)) &= \text{Var}(\alpha(0))e^{2(\lambda-1)\tau} + \frac{\lambda(e^{2(\lambda-1)\tau}-1)}{2(\lambda-1)}. \end{aligned} \tag{S19}$$

Since $\alpha(\tau)$ is a Wiener process (linear superposition of Gaussian noises), $\alpha(\tau)$ follows a Gaussian distribution with mean $\langle\alpha(\tau)\rangle$ and variance Var($\alpha(\tau)$) during the linear amplification stage. In other words, $P\left[\alpha(\tau_0)\right]$ is a Gaussian distribution. Therefore, Supplementary Equation S16 corresponds to the right side integral of the Gaussian distribution for $\alpha(\tau_0) > T(b)$.

$$p = P\left[\alpha(\tau \to \infty) > 0\right] = \frac{1}{2}\left[1 + \text{erf}\left(\frac{-T(b)}{\sqrt{2}\sigma}\right)\right]. \tag{S20}$$

σ in Supplementary Equation S20 is the standard deviation of the Gaussian distribution at τ_0. $T(b)$ is the position of α at τ_0, which becomes $\alpha_{\text{threshold}}$ at τ. Because the field probability distribution broadens while maintaining the Gaussian distribution during the linear amplification stage, the ratio between $T(b)$ and σ is kept constant. Therefore, we can simply set $\tau_0 \to 0$ and calculate $T(b)$. Standard deviation σ at $\tau_0 \to 0$ becomes the standard deviation of the quantum vacuum state, which is $1/\sqrt{2}$ along Re(α) axis.

B. Reconstructing the full dynamics of quantum vacuum state

Supplementary Figure S2 illustrates how we can visualize the amplification of the DOPO signal by analyzing the bias – probability relationship at different time, including the nonlinear absorption stage. As the bias injection is delayed, the probability becomes less sensitive to changes in the bias field (Supplementary Figure S2(a)). To reconstruct the field probability distribution at different time step, we use the bias – probability relationship derived in the previous section for the nonlinear absorption stage, combined with the results from the Methods section of the main text for the linear amplification stage. In Supplementary Figure S2(b), we compare the reconstruction result (blue line) with the field probability distribution of DOPO cavity states numerically calculated from the SDEs (red histogram). The orange solid line shows the analytical solution.

All three solutions show good agreement, demonstrating that we can successfully visualize the amplification and the bifurcation of the cavity state from the bias – probability relationship. Note that the numerical reconstruction is limited in the range of $|\alpha| < \alpha_{\text{critical}} = \alpha_0/\sqrt{3}$ as we cannot reconstruct the dynamics of the DOPO beyond $\alpha_0/\sqrt{3}$ from the bias – probability curve.

C. Generation and collapse of squeezed vacuum state

In Supplementary Equation S6, we solved the dynamics of the OPO with quantum vacuum state as an initial condition. We can extend this concept to reconstruct the dynamics of an arbitrary initial state. Here, we solve the generation and collapse of the squeezed vacuum state (Supplementary Figure S3)

$$P[Z(\tau) \geq 0] = P\left[Z(0) + \sqrt{2}b_0\frac{1-e^{-(\lambda-1)\tau}}{\lambda-1} + \sqrt{\lambda}\int_0^\tau \eta(\tau')e^{-(\lambda-1)\tau'}d\tau' \geq 0\right]. \tag{S21}$$

For the squeezed vacuum state, the initial probability distribution of $Z(0)$ follows the Gaussian distribution with the standard deviation of σ_Z, which now depends on the phase of the amplification (i.e., σ_Z is a function of θ). Therefore, the sensitivity of the bias – probability relationship for the squeezed vacuum state is determined by both the variance of the initial Gaussian distribution and the broadening by the pump.

$$p = \frac{1}{2}\left[1 + \text{erf}\left(\frac{b_0/\sigma_{b0}}{\sqrt{1 + \frac{2{\sigma_Z}^2}{{\gamma_Z}^2}}}\right)\right], \tag{S22}$$

with $\sigma_{b0} \equiv \sqrt{\frac{\lambda(\lambda-1)}{2}}$ and $\gamma_Z \equiv \sqrt{\frac{\lambda}{\lambda-1}}$.

S4. EXPERIMENTAL SETUP

The details of the experimental setup can be found in the Methods section of the main text. The complete experimental setup is shown in Supplementary Figure S4, which is extended from the setup demonstrated in Ref. [2]. Here we focus on two factors that should be considered while modeling our experimental setup in numerical simulations: the finite rise time and the finite extinction ratio of the optical signal.

A. Finite rise time of the pump and bias

In our experiment, the modulation signals from the arbitrary waveform generators (AWGs) are amplified by a high-gain voltage amplifier before driving the electro-optical modulators (EOMs). Due to the voltage amplifier's finite bandwidth, we observe a finite rise time of the optical signals passing the EOMs (Supplementary Figure S5(a)). While we assume an instantaneous rise of the pump and bias field (i.e., the modulated optical signal is a perfect square wave) in our reconstruction protocol, the finite rise times of the pump and bias are considered when we reconstruct the cavity state from the experimental results.

B. Finite extinction ratio of the optical field

When introducing a time delay between the bias and the pump, the bias signal should ideally be fully attenuated during the off state of the modulation. However, EOMs have a finite extinction ratio (Supplementary Figure S5(b)). As a result, there is a non-zero bias field that is injected into the cavity before the bias modulation is turned on. Similarly, the pump field is not completely extinct when the modulation signal is turned off, which introduces a small amplification to the initial cavity quantum vacuum state.

S5. RECONSTRUCTING THE DYNAMICS OF A REALISTIC OPO

In the previous section, we introduced two factors that should be considered when reconstructing cavity quantum states from our experimental results. In this section, we apply these conditions to the numerical simulations and compare to the experimental results.

A. Reconstruction of 1D amplification in the realistic DOPO model

Supplementary Figure S6 shows the amplification behavior of the quantum vacuum state measured with our experimental setup, which deviates from the ideal DOPO case. Under ideal conditions, the standard deviation σ_{b} of the bias – probability sensitivity curve (dp/db) increases exponentially with the time delay. However, experimental results reveal two key deviations, 1) σ_{b} increases slowly at the beginning, and 2) σ_{b} plateaus at a later stage.

Initial slow increase: σ_{b} increases slowly due to the finite rise time of the pump field, resulting in a smaller effective pump field entering to the cavity during the early stage.

Plateau at the later stage: When the time delay between the bias and the pump is significant, the cavity state is displaced by the residual bias field that could not be completely attenuated by the EOM. Therefore, the bias – probability curve becomes independent of the bias injection time once the pump field exceeds the threshold.

To model these effects, we can modify the SDEs as follows:

$$\frac{dX}{d\tau} = (\lambda(\tau) - 1)X + \sqrt{2}b(\tau) + \sqrt{2 - \lambda(\tau)}\eta_X. \tag{S23}$$

Note that we are solving the SDE for the Husimi Q function here. The only difference between the SDEs of the P function and the Q function lies in the noise term. In the realistic model, both λ and b are time-dependent. With the rise time of the pump and bias $T_{p,b}$, extinction ratio of the bias field α, initial and final pump field $\lambda_{0,1}$, and the bias injection time of τ_0, we can write $\lambda(\tau)$ and $b(\tau)$ as :

$$\lambda(\tau) = \begin{cases} \lambda_0 + \frac{(\lambda_1 - \lambda_0)}{T_p}\tau, 0 \leq \tau < T_p \\ \lambda_1, T_p \leq \tau \end{cases} \tag{S24}$$

$$b(t) = \begin{cases} \alpha b_0, 0 \leq \tau < \tau_0 \\ \alpha b_0 + \frac{(1-\alpha)b_0}{T_b}(\tau - \tau_0), \tau_0 \leq \tau < \tau_0 + T_b \\ b_0, \tau_0 + T_b \leq \tau \end{cases} \tag{S25}$$

.

For the experiment in Supplementary Figure S6 and Fig. 3(d) of the main text, $T_p \sim 1.5\tau_{\text{cav}}$, $T_b \sim 3\tau_{\text{cav}}$, $\alpha \sim 0.1$, $\lambda_0 \sim 0.3$, and $\lambda_1 \sim 2.0$. With realistic modeling of the SDEs, the numerical simulation results align with the experimental observations, as shown in Supplementary Figure S6.

B. Reconstruction of 2D phase sensitive amplification in the realistic DOPO model

Supplementary Figure S7 shows how the bias – probability relationship for an amplified quantum vacuum state changes as we rotate the phase of the pump. When $\theta = 90^\circ$, the broadening of the bias - probability curve becomes minimal. While we expect no amplification along $\theta = 90^\circ$ for an ideal DOPO, the finite rise time of the pump field can introduce unwanted broadening in the bias – probability curve. By the time the bias field starts to displace the cavity quantum state along $\theta = 90^\circ$, finite pump field is already introduced, pre-amplifying the orthogonal quadrature. Using our realistic SDE model, we can match the numerical simulation results to the experimental results as shown in Fig. 3(e) of the main text.

This unwanted broadening by the finite rise time of the pump field is also observed when we try to measure the cavity squeezed vacuum state in Fig. 2(f) of the main text. Taking into account of the finite rise time of the pump, we write $Y(\tau)$ as (i.e., quadrature along $\theta = 90^\circ$):

$$\begin{aligned} Y(\tau) = \ & \exp\left(\frac{1}{2}\frac{\lambda_1 - \lambda_0}{T_{\text{p}}}\tau^2 - (1-\lambda_0)\tau\right) \times \\ & \left[Y(0) + \int_0^\tau \exp\left(-\frac{1}{2}\frac{\lambda_1 - \lambda_0}{T_{\text{p}}}t^2 + (1-\lambda_0)t\right)\eta_X\sqrt{2 - \lambda_0 - \frac{\lambda_1 - \lambda_0}{T_p}t}dt\right]. \end{aligned} \tag{S26}$$

Here, we do not consider the effect of the bias because our focus in on how finite rise time of the pump gives an unwanted broadening while measuring squeezed vacuum state. $\text{Var}(Y(0))$

is the actual squeezing we want to measure, while Var$(Y(\tau))$ is the variance of the squeezed vacuum state with unwanted broadening. Because we start from squeezed vacuum state, $\lambda_0 \sim 0.9$, $\lambda_1 \sim 2.0$, $T_\mathrm{p} \sim 1.0$, and τ is defined as the time when $\lambda(\tau) = 1$, which corresponds to the time when the pump field goes above the threshold and determine the probability p.

Using experimental data, we can reconstruct Var$(Y(0))$, estimating a squeezing ratio of $\sim 1.8 \pm 0.7$ dB. Theoretically, we expect ~ 2.7 dB of squeezing for the pump power used in our experiment, assuming instantaneous rise of the pump signal. The underestimation of the squeezing ratio in the experiment can additionally be attributed to the noise of the pump laser.

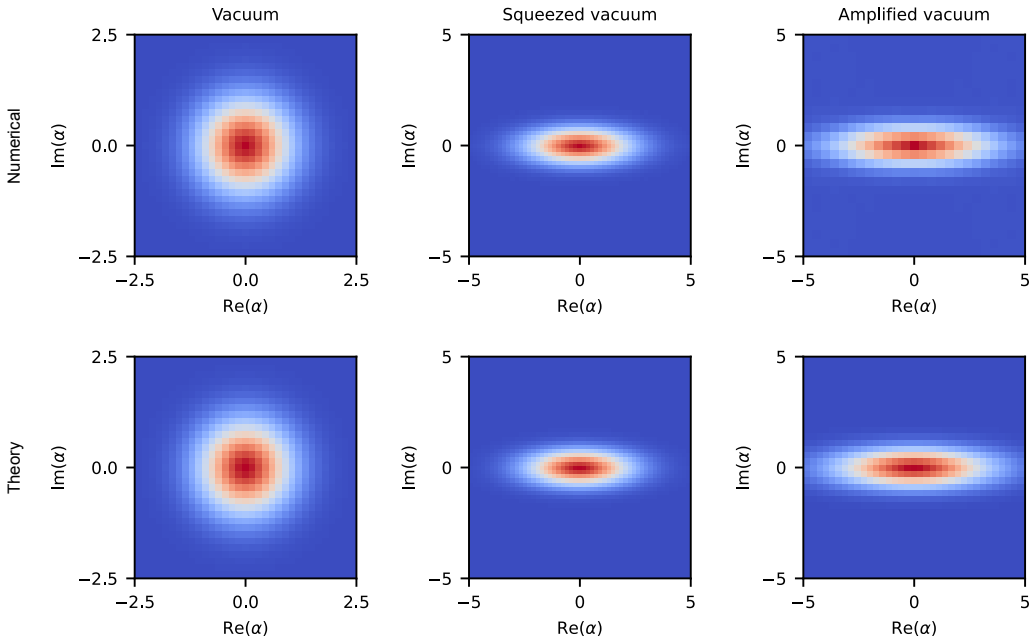

FIG. S1: **Cavity quantum state reconstruction protocol with displacement theorem.** During the reconstruction in numerical experiments, we set $\lambda = 2.0$ to amplify the cavity state along the certain quadrature. The squeezed vacuum state is generated at $\lambda = 0.8$ and the amplified quantum vacuum state is generated at $\lambda = 2.0$ with amplification time $t/t_{\mathrm{cav}} = 1.3$. Then we compare these numerically reconstructed DOPO states to the theory. For quantum vacuum state and squeezed vacuum state, we use the analytical solution. For the amplified quantum vacuum state, we solve the Hamiltonian of the DOPO system and plotted the Husimi Q function.

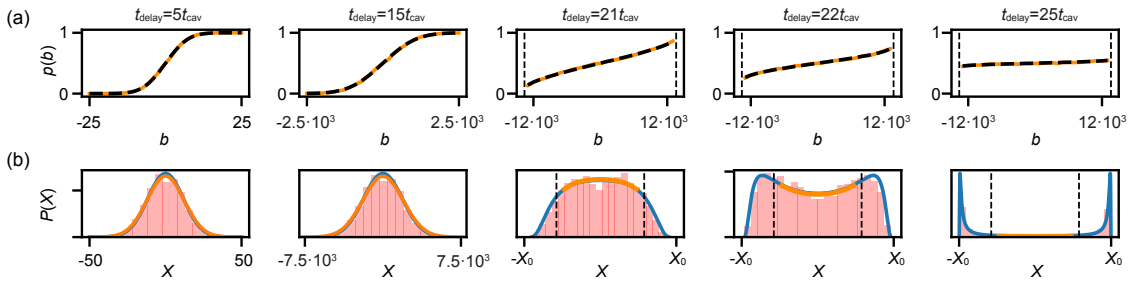

FIG. S2: **Full dynamics of the cavity state inside the DOPO.** (**a**) We solve SDEs for different time steps and measure bias – probability curves (orange curves in the upper panel). We also fit these curves with bias – probability relationships we analytically derived (black dashed curves in the upper panel). (**b**) In the early stage, the field probability distribution gets broaden, which indicates the linear amplification of the cavity state. When the nonlinear absorption becomes apparent, the DOPO undergoes bifurcation process and eventually reaches at the steady state. During the amplification, $\lambda = 1.5$. Red histogram is the numerically simulated field probability distribution using SDEs, orange line is the numerically reconstructed field probability distribution from bias – probability curves, and the blue line is the analytical solution.

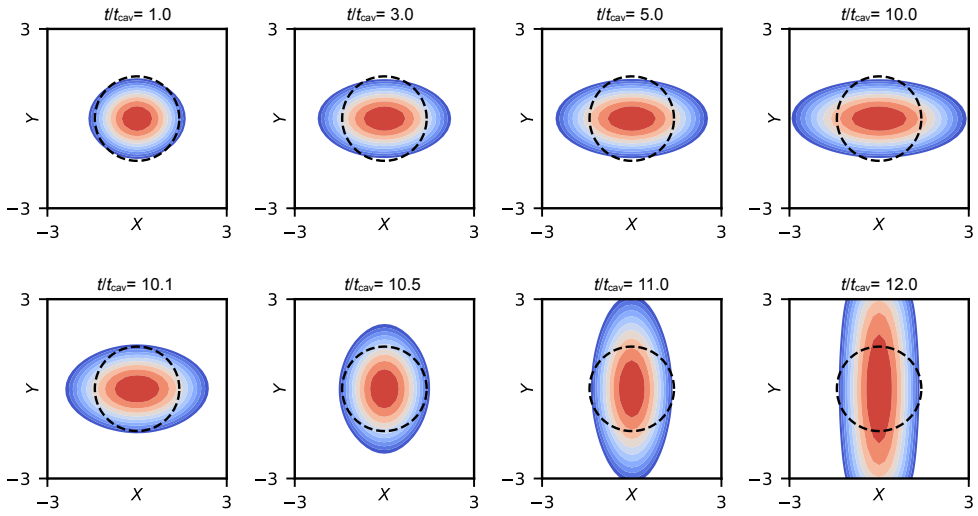

FIG. S3: **Generation and collapse of the squeezed vacuum state inside the DOPO.** The first row shows how the quantum vacuum state can reach at the squeezed vacuum state when pumped at $\lambda = 0.9$. Then we switch the pump field to $\lambda = -1.5$ so amplification happens along the Y quadrature. The dashed circle represents the contour line at 1/e for the quantum vacuum state.

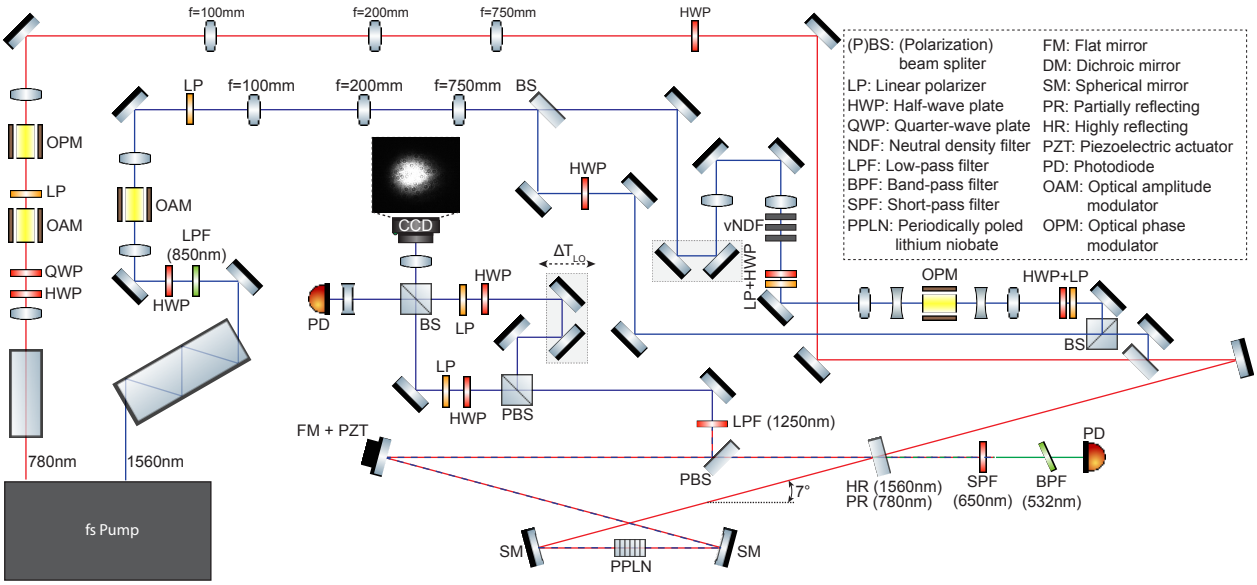

FIG. S4: **Full experimental setup.** The meaning of each acronym is listed on the right side of the figure.

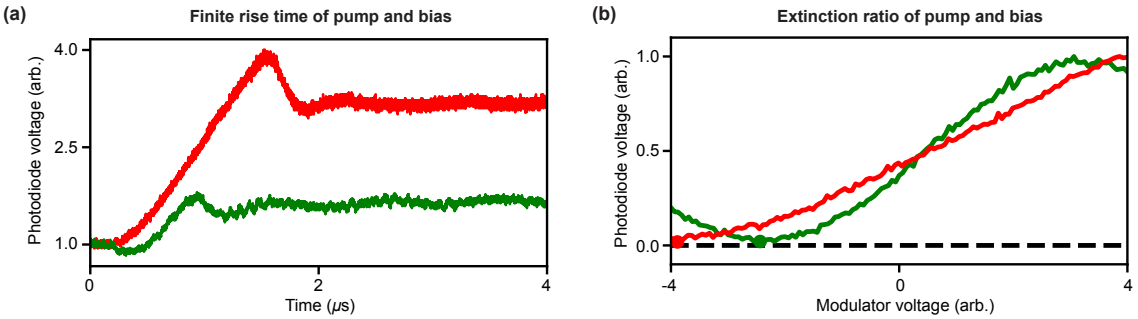

FIG. S5: **Realistic DOPO models.** (**a**) Finite rise time of the pump and bias. The rise time of the pump (green) and the bias (red) are $\sim$450 ns and $\sim$900 ns respectively. (**b**) Finite extinction ratio of the pump and bias. We sweep the modulator voltage and measure the minimum and the maximum photodiode voltage. In this plot, maximum is normalized to 1 and minimum for each signal is marked as a dot. The extinction ratio of the pump (green) and the bias (red) are $\sim$39 dB and $\sim$20 dB in power.

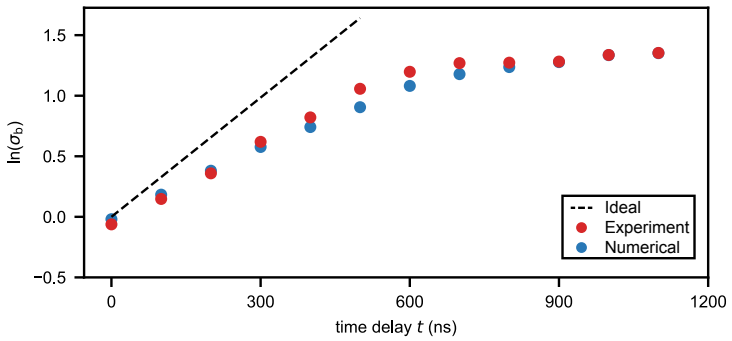

FIG. S6: **1D Amplification of a realistic DOPO model.** The finite rise time of the pump makes the DOPO cavity state to amplify slowly compared to the ideal case. The finite extinction ratio of the bias preseeds the dynamics of the DOPO before the actual bias is injected, saturating the sensitivity of the bias – probability curve when the bias is significantly delayed.

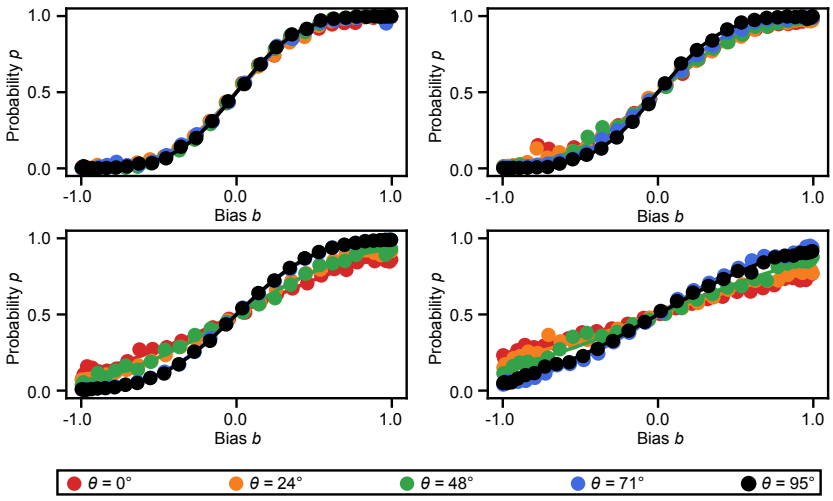

FIG. S7: **Phase sensitive amplification of the DOPO.** The amplification is maximized when $\theta = 0°$.

[1] Carmichael, H. J. *Statistical methods in quantum optics 2: Non-classical fields* (Springer Science & Business Media, 2007).

[2] Roques-Carmes, C. *et al.* Biasing the quantum vacuum to control macroscopic probability distributions. *Science* **381**, 205–209 (2023).

[3] Deans, S. R. *The Radon transform and some of its applications* (Courier Corporation, 2007).